Available online at www.sciencedirect.com
ScienceDirect
Marine Chemistry 105 (2007) 258–270
MARINE CHEMISTRY
www.elsevier.com/locate/marchem

Variability of the apparent quantum efficiency of CO photoproduction in the Gulf of Maine and Northwest Atlantic

Lori A. Ziolkowski, William L. Miller *

Department of Oceanography, Dalhousie University, Halifax, Nova Scotia, Canada B3H 4J1

Received 26 July 2006; received in revised form 1 February 2007; accepted 12 February 2007
Available online 22 February 2007

Abstract

The photochemical oxidation of colored, dissolved organic matter (CDOM) is important for carbon cycling in the ocean. This oxidation process produces a number of products, including carbon monoxide (CO). While the photochemical production efficiency of CO (apparent quantum yield, AQY, defined in terms of CDOM absorbance) has been reported to be similar for many water types, a full evaluation of the observed natural variability in CO AQY requires additional study. Here we use a polychromatic irradiation system to determine twenty AQY spectra at sea on fresh samples ranging from the near coastal waters of the Gulf of Maine to the offshore waters of the Northwest Atlantic. Despite the geographic variability of these marine samples the AQY of CO production in the Gulf of Maine and Northwest Atlantic exhibited only a small degree of variability, none of which was not correlated with measured environmental parameters. Consequently, a single aggregate AQY spectrum $\phi_\lambda = e^{(-(9.134+0.0425(\lambda-290)))+e(-(11.316+0.0142(\lambda-290)))}$ was found to adequately represent the entire data set. Significantly, the accuracy of an AQY spectrum determined using this multispectral/statistical technique was confirmed with data obtained from a monochromatic irradiation technique on a single open ocean sample. Taken together, the AQY spectra determined in this study were similar in magnitude and shape to those previously published for marine samples and, overall, were somewhat lower than those previously reported for freshwater studies.

Keywords: Carbon monoxide; Photochemistry; Dissolved gases; CDOM; Quantum yield; Absorption spectra; USA; Gulf of Maine; NW Atlantic

1. Introduction

Photochemical degradation of colored dissolved organic matter (CDOM) in natural waters results in the formation of a number of products. Since not all photons absorbed by CDOM contribute to photochemical reactions, any specific reaction must be quantified in terms of its efficiency. This measure of efficiency, termed the quantum yield, is defined as the ratio of the moles of product formed (or reactant lost) to the moles of photons of wavelength (λ) absorbed. In natural waters, defining a direct relationship between the primary chromophore and the many resulting photochemical products is difficult, thus the efficiency of such reactions is often referred to as the *apparent* quantum yield (AQY) since the molar absorption coefficient is unknown.

One of the major volatile photoproducts of CDOM degradation is carbon monoxide (CO). For decades it has been reported that CO is produced in surface waters of the ocean (Swinnerton et al., 1970; Conrad et al., 1982; Zafiriou et al., 1984, Jones, 1991, Kettle, 1994; Ohta, 1997). However, there have been relatively few

* Corresponding author. Department of Marine Sciences, University of Georgia Athens, Athens, GA, 30602.
E-mail address: bmiller@uga.edu (W.L. Miller).

0304-4203/$ - see front matter © 2007 Elsevier B.V. All rights reserved.
doi:10.1016/j.marchem.2007.02.004

AQY spectra reported for the production of CO. CO apparent quantum yield data have been reported for a number of high carbon inland river and lakes (Valentine and Zepp, 1993; Gao and Zepp, 1998), the low carbon waters of the Sargasso Sea (Kettle, 1994), coastal waters in England (Stubbins, 2001) and most recently for the Pacific Ocean (Zafiriou et al., 2003). The AQY spectra published by Valentine and Zepp (1993) and Gao and Zepp (1998) are higher than those presented by Kettle (1994), suggesting terrestrially derived CDOM may exhibit different efficiency for producing CO than marine derived CDOM. Zafiriou et al. (2003) found that the apparent quantum yield for a number of regions in the north and south Pacific did not exhibit strong regional variations. The AQY spectra reported for the Pacific were quite similar to those reported by Kettle. It was noted in Zafiriou et al. (2003) that although a number of different regions in the Pacific were sampled, most of the CDOM sampled was likely of marine origin since most riverine CDOM discharges into the Atlantic and Arctic rather than the Pacific Ocean (Opsahl and Benner, 1998; Amon et al., 1999). These studies suggest that terrestrial DOM may be more efficient at producing CO than oceanic CDOM. If this is true, then the apparent quantum yield spectra for CO in coastal waters, which contain a mixture of terrestrial and oceanic CDOM, should fall between the apparent quantum yield spectra for inland waters and those of offshore waters.

This paper presents twenty CO AQY spectra from a transect of different water types (coastal, shelf and offshore) collected in the Gulf of Maine, Northwest Atlantic and Sargasso Sea. Here we also describe a multi-spectral irradiation system that allows rapid determination of CO AQY spectra on fresh samples at sea.

2. Methods

2.1. Site description

Samples were taken from the coastal and shelf waters of the Gulf of Maine, Northwest Atlantic and the Sargasso Sea (Fig. 1, Table 1). All samples except those in the Sargasso Sea were collected using 15 L Niskin bottles and were gravity filtered (0.2 μm Millipore Polycap 75 AS nylon membrane) directly into acid washed rinsed 1 L amber glass bottles. Water samples from the Sargasso Sea for AQY determinations were collected using the shipboard rosette outfitted with 5 L titanium bottles (Woods Hole Oceanographic Institute), 0.2 μm filtered (Nucleopore®), poisoned with cyanide and purged with CO-free air prior to being sub-sampled into irradiation vessels. Samples for absorption spectra were taken from the Sargasso Sea using 15 L Niskin bottles and 0.2 μm filtered (Nucleopore® filters).

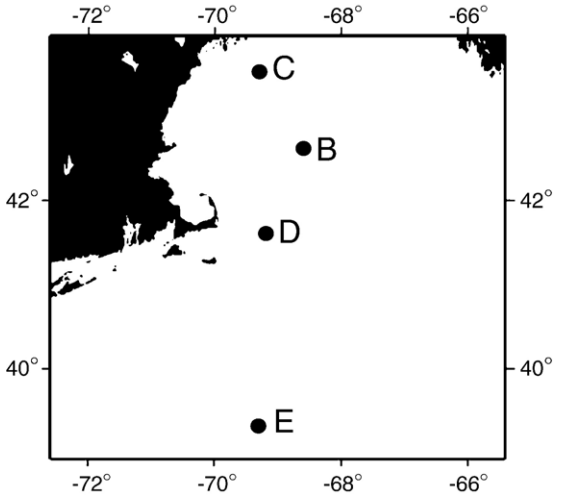

Fig. 1. Sample stations for this study. Station Id's are as follows: B = Ammen Rock (shelf waters), C = Damariscotta Estuary (coastal), D = shelf water and E = Oceanographer's Canyon (offshore). Not shown on this map is the Sargasso Sea station south of Bermuda.

2.2. CDOM absorption spectra

For all samples from the Gulf of Maine and the Northwest Atlantic, water was brought to room temperature and sonicated for 5 min to remove excess air before the absorbance was measured (HP 8453 UV–Vis from 250 to 800 nm) using a quartz 5 cm flow-through cell. All samples were optically thin (absorbance less than 0.05 cm^{-1} at 350 nm), such that there was a constant light intensity throughout the cell, precluding significant self-shading. The absorption coefficient ($a_{CDOM}(\lambda)$, m^{-1}) was calculated from the absorbance ($A_{CDOM},(\lambda)$ unitless):

$$a_{CDOM}(\lambda) = \frac{2.303 A_{CDOM}(\lambda)}{z} \quad (1)$$

where z is the path-length (m) of the absorption cell and 2.303 converts from the log base ten of the spectrophotometer measurements to natural log (Braslavsky et al., 1996). No detectable fading was observed in irradiated samples.

A correction for scattering, index of refraction differences and blank drift was applied to all samples by fitting the measured absorption (280–800 nm), with the MATLAB nlinfit.m subroutine to an equation of the form

$$a_{CDOM}(\lambda) = Ce^{-S\lambda} + a_o \quad (2)$$

Table 1
Characteristics of samples studied in this work

Sample label	Latitude (N, W)	Longitude	Water types	Temperature (°C)	Salinity (psu)	Depth (m)	a_{350} (m^{-1})	Production rate [a] (nmol L^{-1} h^{-1})	a_{350} normalized production rate (nmol m L^{-1} h^{-1})
190B12	42.6°	68.6°	Shelf	19.2	32.0	3	0.40	3.66	9.14
191B11	42.5°	68.4°		6.4	32.6	80	0.32	5.21	16.29
192B1110	42.5°	69.0°		5.1	32.8	100	0.36	5.22	14.49
192B1118	42.5°	69.0°		14.0	32.1	18	0.41	2.61	6.36
193B02	42.5°	69.0°		13.8	32.2	20	0.44	6.87	15.61
193B23	42.5°	69.0°		12.2	32.1	21	0.42	6.20	14.76
202D11s	41.6°	69.2°		17.3	32.0	10	0.41	9.95	35.53
202D11d	41.6°	69.2°		5.8	33.3	150	0.28	9.94	24.26
195C11b [b]	43.5°	69.3°	Coastal	12.8	31.6	12	0.85	11.91	14.01
195C11a [b]	43.5°	69.3°		12.8	31.6	12	0.85	12.01	14.14
196C11	43.5°	69.3°		12.1	31.6	10	0.79	12.20	15.44
199C11	43.5°	69.3°		10.2	31.7	20	0.72	12.70	17.64
201C02	43.5°	63.3°		10.8	31.7	18	0.69	10.81	15.67
201bk (n=3)	43.5°	63.3°		–	–	<1	0.69		
204E11	39.4°	69.3°	Offshore	24.0	36.0	30	0.05	1.65	32.9
205E11	39.4°	69.3°		19.1	35.4	60	0.13	3.61	27.76
206E02	39.3°	69.3°		17.0	35.6	80	0.17	2.59	15.22
206E23 [c]	39.3°	69.3°		24.6	35.2	<1	0.17	2.27	13.35
Sargasso [d]	32.0°	64.5°			36	20			

Sample names begin with three numbers (Julian day of sample collection) followed by a letter (the Station ID) and two digits (nearest hour to when sample was collected UTC). Station Id's are as follows: B = Ammen Rock (shelf waters), C = Damariscotta Estuary (coastal), D = shelf water, E = Oceanographer's Canyon (offshore), and bk = bucket samples taken at station C.

[a] Average production rate from two measurements taken from two samples exposed to light at wavelengths greater than 295 nm.

[b] Duplicate samples.

[c] Absorbance data for 206E23 was lost and 206E02 was used in its place.

[d] The Sargasso sample is an aggregate of three samples.

where C (m^{-1}), a_o (m^{-1}) and S (nm^{-1}) are fitting parameters, the later defining how rapidly the absorption coefficient decreases with increasing wavelength (Blough and Del Vecchio, 2002 and references therein). The offset, a_o, was then subtracted from the whole a_{CDOM} spectrum to give the corrected spectrum used in subsequent calculations. The corrected spectra were then refit using Eq. (2) and the MATLAB nlinfit subroutine over the more limited spectral range of 280–700 nm to derive the $S_{280-700}$ values reported in Section 3.1. While these $S_{280-700}$ values are almost identical to the 'S' parameters found in the original fit of the absorbance spectra, they were deemed to be more compatible to other "CDOM Slope" values reported in the literature. Samples collected in the Sargasso Sea were stored at 4 °C and were analyzed in the lab, back on land, by allowing samples to warm to room temperature in the dark before measuring the absorption spectra with a dual beam Perkin-Elmer Lambda 18 spectrophotometer using a 10 cm quartz cell. A blank scan (Milli-Q water versus Milli-Q water) was subtracted from each spectrum.

2.3. CO irradiations

To generate the photochemical CO production rates for use in the AQY calculations, all lab irradiations (2 to 6 h in length) were conducted at sea using a Suntest CPS Solar Simulator equipped with a 1.5 kW xenon burner tube (Atlas, Chicago, Il, USA), as described in detail by Johannessen and Miller (2001). Experiments with samples from the Gulf of Maine and Atlantic (collected July, 1999) were accomplished by simultaneously irradiating 15 hand-made, gas tight, air-cooled quartz cylinders (5.4 cm long, 2.3 cm in diameter, flat windows on each end for irradiation, side arms for septa and filling vent) sealed using 20 mm silicone septa with aluminum tear away seals under the xenon lamp. The cylindrical sides of each quartz tube were wrapped in black electrical tape. Samples from the Sargasso Sea (collected March, 2000) were irradiated in 10 cm quartz spectrophotometer cells, supported in a water-cooled aluminum block which did not allow light to pass between cells. Samples were maintained at 20 °C for the duration of

the irradiation (5 h on average). The quartz cylinders were positioned vertically under long-band-pass cut-off filters (Schott models WG 280, WG 295, WG 305, WG 320, WG 335, WG 345, GG 385, GG 425, GG 480; Oriel) and supported on a piece of black felt. The spectral irradiation intensity under each cut-off filter was measured at 1 nm intervals from 250 to 800 nm using an Optronic OL 754 spectroradiometer (Orlando, FL, USA) outfitted with a fiber optic cable with a terminal Teflon diffuser. Spectrally similar to sunlight prior to passing through our optical filter set (Johannessen and Miller, 2001), the total radiation flux (280 to 700 nm) under the WG 280 and GG 480 cut off filters was 200.53 mol photons m^{-2} s^{-1} and 66.90 mol photons m^{-2} s^{-1} respectively. The spectroradiometer, configured exactly as implemented in these experiments, was calibrated using an Optronic OL 752-10E irradiance standard. Successive measurements with the Optronic showed less than 1% variation in irradiance at any wavelength. To account for photon loss at the quartz window a spectral transmittance correction was applied to each sample.

After irradiation, a known volume of CO-free air was added to each irradiation cell, displacing an equivalent volume of seawater. The CO free air was generated by passing room air through a column containing Schutz reagent (Aldrich). To equilibrate the seawater with the headspace, each cell was shaken vigorously by hand for 1 min and then allowed to sit for 2 min before sampling the headspace. The headspace in the irradiation cell was drawn into a 10 mL syringe without allowing exposure to the atmosphere.

CO in the headspace drawn from the irradiation cells was measured using a Trace Analytical RGA-3 (Trace A, Menlo Park, CA, USA) gas chromatograph. Details of the Trace-A configuration are described in Xie et al. (2002). Briefly, gas samples were injected onto a pair of chromatographic columns at 105 °C to separate the CO from hydrogen. Thirty seconds after the injection, the first column (Unibeads) is back flushed to protect the second column (MolSeive) against contamination while CO and hydrogen are separated and carried to a mercuric oxide bed reactor at 265 °C, where CO quantitatively reduces mercuric oxide to mercury vapour, which is quantified by a UV photometer. The millivolt output was recorded and integrated on a Hewlett Packard Integrator (model 3396A) and results were recorded as peak areas.

While aboard the ship, a nominal "1 ppm" CO standard (Scott Marin) was used to calibrate the instrument. After the cruise, the 1 ppm standard was calibrated against a 10 ppm National Institute of Standards and Technology (NIST) standard and determined to be 1.14 ppm (see Xie et al., 2002) which was used in our calculations. Raw peak areas were converted to aqueous carbon monoxide concentrations (nmol L^{-1}) using a two-part calculation, as described in detail in Xie et al. (2002) that incorporates the following: the Bunsen solubility coefficient, which is a function of temperature and salinity developed by Wiesenburg and Guinasso (1979); atmospheric pressure (millibars); and equilibration temperature (degrees Celsius). In the first step of the calculation, the measured CO concentration in the headspace is used to calculate the CO concentration remaining in the water after equilibration. The second step of the calculation calculates the CO concentration in the initial sample by assuming a mass balance equation, considering the volume of the water and air samples sizes.

Dark controls were used to provide a measure of background [CO] in the samples. Microbial production and consumption of CO was assumed to be insignificant over the course of our experiments as preliminary studies showed no significant change of [CO] over 6 h. Using multiple dark controls, two batches of samples were irradiated to determine the detection limit for measuring the concentration of CO. In these experiments, 6 tubes were wrapped in foil and black felt and placed under the longer wavelength positions (Schott filters GG 380, GG 425 and GG 480) as well as the position that was exposed to no irradiation (dark position). It was established from these experiments that our CO detection limit was 0.9 nmol L^{-1} (defined as three times the standard deviation of the blanks). The average hourly CO production rate (nmol L^{-1} h^{-1}) under the 295 nm cut-off filter was 8 times the detection limit.

2.4. Calculating the spectral apparent quantum yield

Using a measured photochemical production rate for CO, the CDOM absorption coefficient spectra and the incident spectral irradiance for each exposed tube, the apparent quantum yield spectra can be calculated. The rate of a given photochemical reaction (dP/dt, mol m^{-2} s^{-1}) can be expressed by:

$$\left(\frac{dP}{dt}\right) = \int_{280}^{700} (\phi(\lambda) E_a(\lambda)) d\lambda \quad (3)$$

where $\phi(\lambda)$ refers to the wavelength dependent quantum yield, and $E_a(\lambda)$ refers to the spectral photon absorption rate in the sample (moles photons m^{-2} s^{-1} nm^{-1}). We used an expanded form of Eq. (3) which corrects the

calculation for self-shading in the sample and assumes insignificant absorption of UV by water relative to CDOM as discussed in Hu et al. (2002),

$$\left(\frac{dP}{dt}\right) = \int_{280}^{700} (\phi(\lambda)E_o(\lambda)(1-e^{-a_{CDOM}(\lambda)}(Ar/V)))d\lambda \quad (4)$$

where Ar/V is the irradiated area to total volume ratio of the sample (m^{-1}), $E_o(\lambda)$ refers to incident irradiance (mol m^{-2} s^{-1} nm^{-1}) and $a_{CDOM}(\lambda)$ is the absorption coefficient (m^{-1}).

Quantum yield ($\phi(\lambda)$) is traditionally defined as the ratio of the number of molecules transformed via one reaction pathway to the number of photons absorbed by the reactant at a given wavelength. Neither the molar absorption coefficient of the chromophores driving CO photochemistry nor the specific reaction mechanisms for CO production in seawater are known with certainty. Consequently, we define the AQY as follows:

$$AQY_\lambda = \frac{\text{CO produced (moles } m^{-3}s^{-1})}{\text{photons absorbed by CDOM in sample (moles } m^{-2}s^{-1}nm^{-1})}. \quad (5)$$

The AQY spectra presented here were calculated using an iterative curve fitting method, described by Rundel (1983). Using the measured spectral absorption coefficients, spectral irradiance and the production of CO in Eq. (4), a statistical solution was obtained for AQY_λ with an in-house MATLAB® routine (original code by R. Davis, Dalhousie University, Canada) based on Rundel's statistical approach for the optimization of action spectra (Rundel, 1983; Cullen and Neale, 1997; Johannessen and Miller, 2001; Miller et al., 2002).

A caveat of this method is that the AQY is required to have a shape defined by a specific mathematical function. Initially, since many previously published spectral AQYs for products resulting from CDOM photoxidation behave according to a decreasing exponential (e.g.: dissolved inorganic carbon (Johannessen and Miller, 2001), CO (Kettle, 1994; Stubbins, 2001), hydrogen peroxide (Andrews et al., 2000)), a single exponential was used to fit the data of the form:

$$AQY(\lambda) = \exp`-(m1 + m2(\lambda-290))) \quad (6)$$

where λ is wavelength (nm) and $m1$ and $m2$ are the best-fit parameters. The MATLAB® routine iteratively alters the fitting parameters ($m1$ and $m2$) from the initial estimates minimizing the difference between the measured production values and those predicted by the photochemical rate equation (Eq. (3)) with AQY from Eq. (6). To investigate the possibility of a superior fit of data, other exponential based equations were also applied, including a double exponential,

$$AQY(\lambda) = \exp(-(m1 + m2(\lambda-290) + m3(\lambda-290)^2) \quad (7)$$

and a two-part single exponential

$$AQY(\lambda) = \exp(-(m1 + m2(\lambda-290)) + \exp(-(m3 + m4(\lambda-290)). \quad (8)$$

Agreement between predicted and measured CO production values using the single exponential fit for AQY were very good, with r^2 values ranging from 0.90 to 0.99 for 19 of 20 irradiations (~28 data points per irradiation, 2 injections per tube and 14 tubes). The comparison of measured CO production values to calculated values for the best and worst fits obtained from the 19 AQY determinations is shown in Fig. 2. The first sample irradiated during the cruise, sample 190b12, was not irradiated long enough to produce significant CO for confident measurement in the majority of sample tubes, gave a poor r^2 value ($r^2=0.80$) for AQY, and thus was omitted from further calculations.

3. Results and discussion

3.1. CDOM spectra

Significant changes in the magnitude and shape of measured CDOM absorption spectra were observed from offshore to near shore sites, similar to results presented in Vodacek et al. (1997). These results are shown in Fig. 3. Coastal samples (Damariscotta Estuary, Gulf of Maine) had high UV absorption coefficients and the lowest spectral slope coefficients (S as calculated from absorbance spectra by Eq. (2); e.g. sample: 193b02, $S_{280-700}=0.0185$), while offshore samples (Oceanographer's Canyon, Northwest Atlantic) exhibited the smallest UV absorption coefficients and highest spectral slope coefficient values (e.g.: sample: 204e11, $S_{280-700}=0.0239$). The offshore increase in S may reflect different source(s) and/or irradiation history of the CDOM and consequently could correlate to photochemical reactivity of CDOM.

3.2. Photochemical production rates

By using 14 separate quartz tubes under a variety of long band pass cut-off filters, each experiment yielded 14 distinct photochemical production rates corresponding

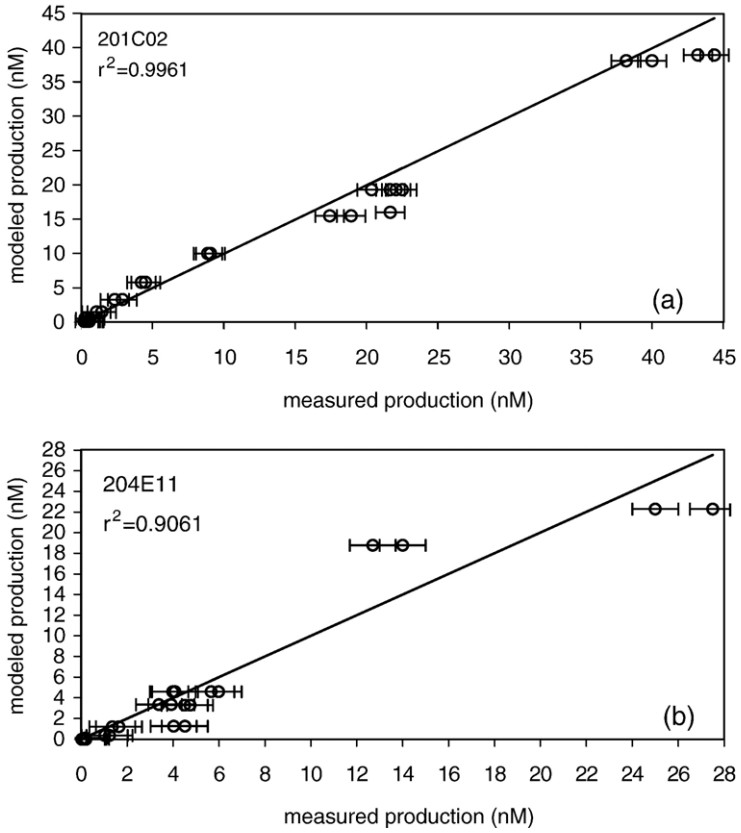

Fig. 2. Representative comparisons of calculated and measured CO photoproduction in irradiated sample cells with our best (a) and worst (b) fits using the single exponential equation: (a) sample 201C02 (r^2=0.99); (b) sample 204E11 (r^2=0.91). One-to-one lines show where the calculated values would fall if they reproduced the measured values exactly. Error bars are the ±0.9 nM CO analytical detection limit.

to different exposure wavelengths and intensities. Consequently, it is difficult to present all of our measured rate data, as is typically done for monochromatic or full spectrum irradiations. To attempt a comparison of our data with previous studies, such as Valentine and Zepp (1993) who presented near-surface production rates for riverine samples, the total dark corrected photoproduction rates from the 295 nm cut-off filter (Schott WG 280) from this study are presented in Table 1. These values are not corrected for self-shading since a calculation of this potential effect on our darkest sample indicated it to be less than 5%. The 295 nm cut-off filter CO production rates from all stations, which ranged from 2 to 13 nmol L^{-1} h^{-1}, proved to be well correlated (r^2=0.73) with the measured absorption coefficient (m^{-1}) at 350 nm (a_{350}) as shown in Fig. 4. The magnitude of absorption coefficient and CO production rate values presented here are up to 100 fold smaller than the freshwater data presented by Valentine and Zepp (1993), however once CO production rates were normalized to the a_{350} (Table 1), our average normalized production rate, (17.80±7.83 nmol m L^{-1} h^{-1}), is in the same range as the a_{350} normalized average production rate (12.93± 3.17 nmol m L^{-1} h^{-1}) of Valentine and Zepp (1993). The strong correlation observed between CO production

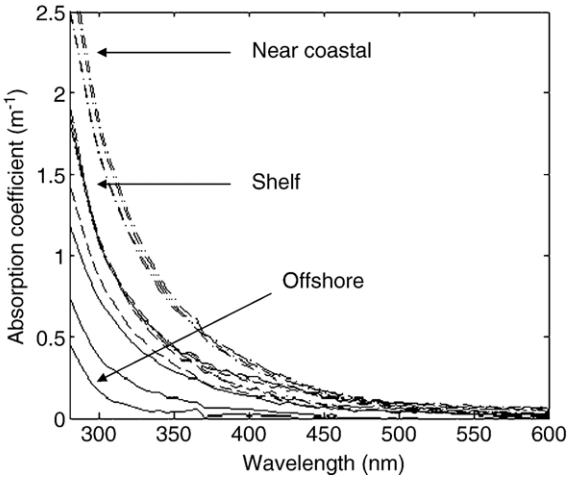

Fig. 3. Range of the measured absorption spectra in the Gulf of Maine and Northwest Atlantic Ocean in July, 1999 (n=19).

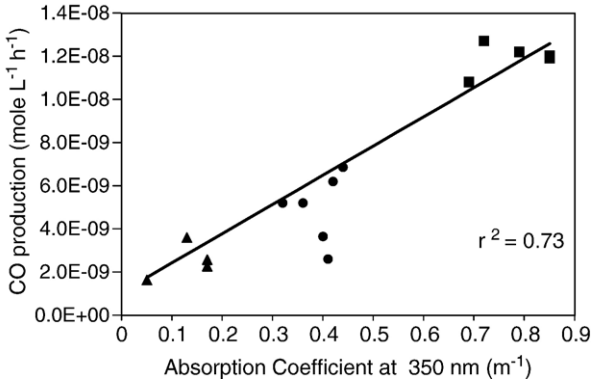

Fig. 4. CO photoproduction under the 295 nm cut-off filter versus a_{350}. Samples taken at the coastal station (Damariscotta River) are represented by squares, shelf water samples (Ammen Rock, station D) are represented by circles and triangles represent samples taken at the offshore station (Oceanographer's Canyon).

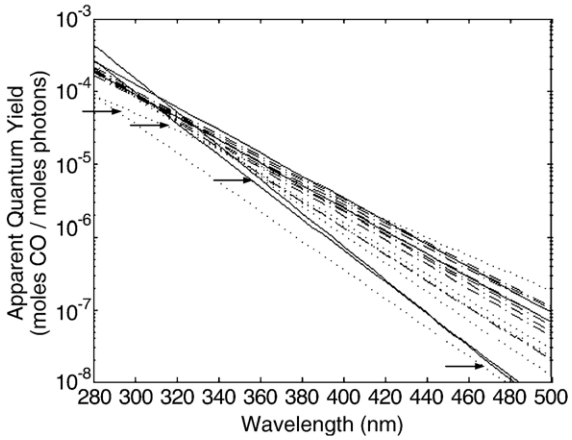

Fig. 5. Apparent quantum yield spectra for the photochemical production of CO measured from 20 samples in the Gulf of Maine and Northwest Atlantic. Samples indicated with an arrow are samples that were excluded from analysis when making group calculations.

rates and a_{350} in our samples is also like those reported by Valentine and Zepp (1993). However, the magnitude of these observations can neither be directly compared nor used for speculation as to the similarity of CO AQY spectra in different water types since the experimental irradiance used for the two experiments cannot be shown to be of the same intensity and/or spectral shape.

Once the CO production rates were determined, they were coupled with CDOM spectra and irradiation spectra to calculate the spectral AQY using the mathematical form of a single exponential. A graphical summary of these AQY spectra is shown in Fig. 5 and the resultant m-values (as per Eq. (6)) along with correlation coefficients are shown in Table 2. The correlation coefficient of an AQY spectrum is determined by calculating the difference between the modelled CO production rates (Eq. (4)) with those measured experimentally. Although the correlation of the single exponential AQY spectra were quite high (r^2=0.90–0.99), the validity of this fit was investigated further for the following reasons: 1) previous studies (Kettle, 1994; Zafiriou et al., 2003) have shown that although a single exponential fit to the CO AQY is accurate in the ultraviolet wavelengths, the accuracy of the fit deteriorates in the visible wavelengths, and 2) it is possible to yield high correlation coefficients for the single exponential, when not fitting the visible production rates accurately since the high production rates in the UV region can drive the statistical fit. Based on these two observations other mathematical fits for the CO AQY were investigated. The double exponential,

$$\phi(\lambda) = e^{-(m1+m2(\lambda-290)+m3(\lambda-290)^2)} \quad (9)$$

was rejected as a general "best fit" for the AQY spectra of CO after the modelled AQY spectrum for some samples were found to increase with increasing wavelengths (in the visible), contrary to physical data. The two-part exponential, requiring four parameters, was not fully constrained by the limited number of data points from an individual experiment. Thus using our

Table 2
Apparent quantum yield fit parameters for the single exponential equation: $\phi_\lambda = e^{(-(m1+m2(\lambda-290)))}$

Sample name	$m1$	$m2$	r^2	Average r^2 for each water type	IPR [a] (pmol CO L^{-1})
190B12	9.616	0.028	0.796	0.978	2.248
191B11	8.977	0.040	0.958		2.551
192B11D	9.011	0.041	0.958		2.375
192B11S	9.779	0.046	0.988		0.919
193B02	8.788	0.045	0.989		2.564
193B23	8.878	0.042	0.990		2.613
202D11s	8.505	0.040	0.995		4.091
202D11d	8.751	0.041	0.970		3.080
195C11B	8.967	0.038	0.993	0.989	2.786
195C11A	9.035	0.036	0.988		2.821
196C11	9.040	0.034	0.991		3.051
199C11	8.872	0.034	0.991		3.610
201C02	8.918	0.036	0.996		3.171
201bk10	8.944	0.034	0.980		3.359
201bk16	8.805	0.038	0.988		3.277
202bk00	8.896	0.042	0.987		2.566
204E11	8.268	0.053	0.906	0.947	3.293
205E11	8.624	0.036	0.975		4.255
206E02	8.942	0.036	0.917		3.096
206E23	8.727	0.050	0.990		2.295

r^2 values estimate how well the measured CO production correlates with the calculated CO production using the newly calculated quantum yield.
[a] IPR = integrated photochemical response (see text for explanation).

results, alternative possible equations that might fit the production data more accurately than a single exponential were proved to be unsatisfactory when applied to a single experiment.

3.3. Variation of apparent quantum yield

Previous CO AQY data (Valentine and Zepp, 1993; Kettle, 1994; Gao and Zepp, 1998) showed a large range of variability for waters originating from high carbon freshwaters to low carbon marine waters. Our data set, which consists of coastal, shelf, and blue water samples, offers the potential for a systematic investigation of the spatial variation of the CO AQY spectrum. To evaluate the total variability in the AQY spectrum, accounting for variations in both the $m1$-value (intercept of the regression of AQY versus wavelength) and the $m2$-value (slope of the regressions of AQY versus wavelength), we calculated an "integrated photochemical response" (IPR, pmol L^{-1}, Table 2). This calculation, which is the product of each AQY spectrum multiplied by a reference spectrum for both absorption coefficient and irradiance (Eq. (3)), isolates the role of AQY variability in the photochemical rate equation. The absorption and irradiance measurements used as the reference spectra for this calculation were collected at Ammen Rock (42° N 68° W) on July 12th, 1999. Using irradiance data measured at discrete bandwidths (Satlantic OCI-200, Halifax, Canada) for the sea surface at local noon, the Gregg and Carder (1990) clear sky model was scaled to local conditions to provide a 1 nm resolved irradiance spectrum.

As a preliminary evaluation of the use of routinely measured seawater parameters in understanding AQY variability, the IPR for each sample (determined as described above) was evaluated for its correlation with salinity, original sample temperature, depth of collection and absorption coefficient at 350 nm. None of these parameters showed significant correlation with IPR (all $r^2 < 0.06$, Fig. 6). With no evidence of an obvious regional or spatial AQY trend, we then calculated a single AQY spectrum for the pooled data set. This was accomplished by calculating a single mathematical fit to all CO production, absorption spectrum, and irradiance data for all 19 experiments together, solving for a single equation to describe one AQY spectrum for CO production (referred to here as the aggregate AQY spectrum).

3.4. Aggregate AQY determination

As a first attempt to pool the production data from all the irradiation data in our study, an aggregate AQY was

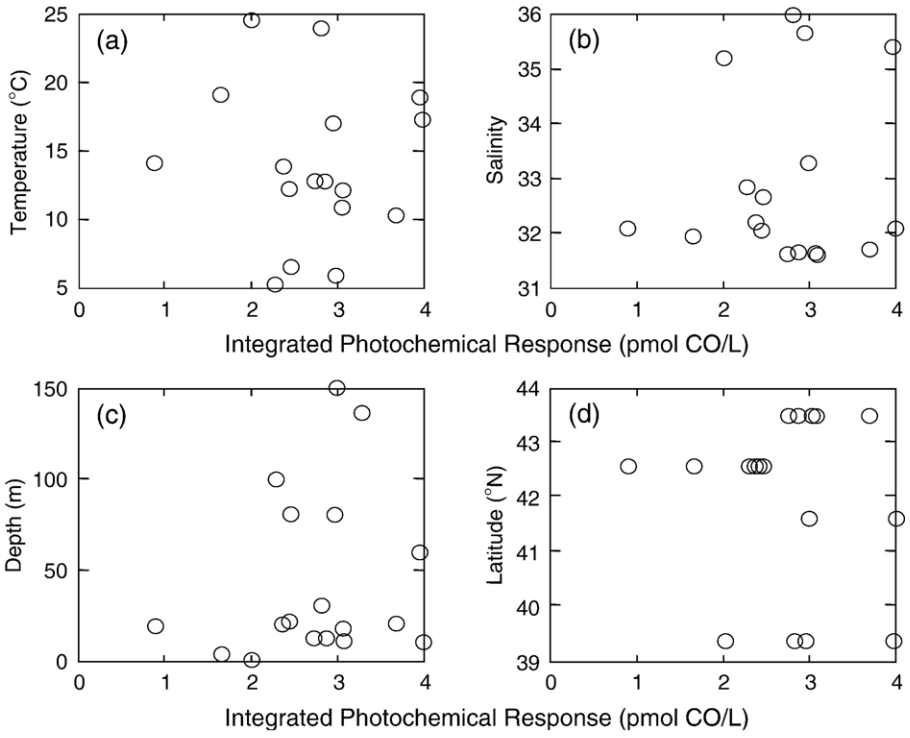

Fig. 6. Integrated photochemical response (IPR), determined using the single exponential AQY spectrum for each sample, as it correlates to (a) sea temperature, (b) salinity, (c) depth, and (d) latitude.

calculated in the form of a single exponential (Fig. 7), as follows:

$$\phi(\lambda) = e^{(-(9.052+0.0415(\lambda-290)))}. \quad (10)$$

Since Kettle (1994), Zafiriou et al. (2003) and Stubbins (2001) all noted that the AQY spectrum that best described their CO data sets consisted of two single exponential curves intersecting near 340 nm, it seemed appropriate to determine whether the aggregate AQY spectrum for our pooled data set shared this characteristic. Due to the nature of our experimental setup and analysis (long bandpass cut-off filters and predefined fitting function), our results would not intrinsically exhibit a bend in the AQY spectrum.

In order to explore the possibility of an AQY spectrum with a bend in the UV-A, all of the CO production rate data were separated into two groups, one from longer and one from shorter wavelength cut-off filters. Independent AQY spectra were calculated for each group. When choosing the wavelength cut-off point for calculation of this two-part quantum yield spectrum, one set of CO production values (from samples irradiated under a given cut-off filter) was chosen for inclusion in both sets to anchor the two AQY spectra together. Initial trials at calculating intersecting AQY spectra for this data set used the production data from the cut-off filters assigned to two groups: (1) 280, 295, 305 and 320 nm, and (2) 320, 335, 345, 380, 425, and 480 nm respectively. The AQY spectra calculated using group 1 (280–320 nm) and group 2 (320–480 nm) yielded the same slope coefficient for the regression of the AQY spectrum versus wavelength ($m2=0.042$), demonstrating that the production data from these chosen wavelength ranges effectively had the same AQY spectrum. However, when the grouping of the data from cut-off filters was shifted to incorporate the 335 nm cut-off in the first group of data and omitting the 320 nm cut-off data from the second group, the resultant AQY spectra exhibited significantly different $m2$-values. Individual AQY spectra were determined for a third grouping with the 345 nm cut-off data chosen for overlap, but this grouping was subsequently rejected as being a valid fit for AQY spectra because the longer wavelength cut-off filter group produced an AQY spectra that increased with increasing wavelength, a result contrary to the measured physical data (i.e. absorption spectrum and production data) used as input to the calculation. The two AQY equations generated from grouping 280–335 nm and 335–480 nm were subsequently added together to yield a full spectrum aggregate AQY equation for the Gulf of Maine and Northwest Atlantic (designated "two-part" in Fig. 7), referred to as our "two-part aggregate" treatment:

$$\phi(\lambda) = e^{(-(9.134+0.0425(\lambda-290)))} + e^{(-(11.316+0.0142(\lambda-290)))}. \quad (11)$$

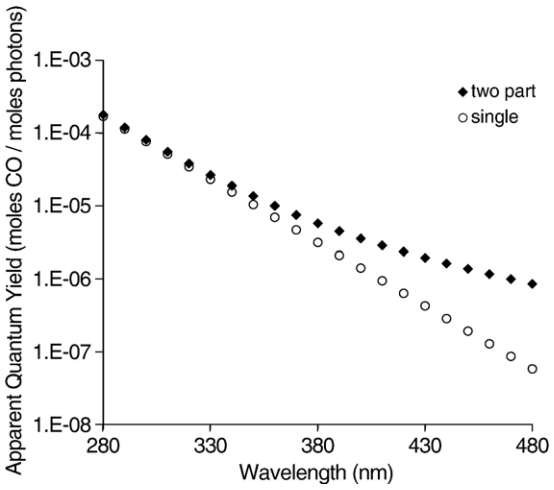

Fig. 7. Comparison of the single exponential aggregate quantum yield spectrum with the two-part aggregate exponential quantum yield spectrum.

Comparing the quantum yield in Eq. (11) to previous monochromatic AQY studies is not straightforward because our statistical fitting method for determining AQY spectra provides a unique equation that plots as a continuous line while monochromatic studies determine the AQY at specific wavebands. However, the monochromatic CO AQY data presented by Zafiriou et al. (2003) from the Pacific Ocean was also analyzed for "one-segment" and "two-segment" treatments similar to the "single exponential aggregate" and "two-part aggregate" approaches used in this study. Zafiriou et al. (2003) plotted the log-linear slope coefficients of AQY spectra versus latitude for data collected over a north–south transect in the Pacific Ocean from 70° S to 40° N and showed that when the AQY was fit with a "one-segment" treatment, the slope of the AQY spectrum becomes less negative as one moves north in the Pacific Ocean. This suggests that the longer wavelengths are more important for CO production in the northern Pacific Ocean than in the south Pacific. The slope coefficients for the Zafiriou et al. (2003) "one-segment" treatment at 40° N in the Pacific (−0.050) is of a similar magnitude to the calculated $m2$-value for our single exponential aggregate AQY ($m2=-0.0415$). For wavelengths less than 360 nm, Zafiriou et al. (2003) showed that there was little correlation between latitude and

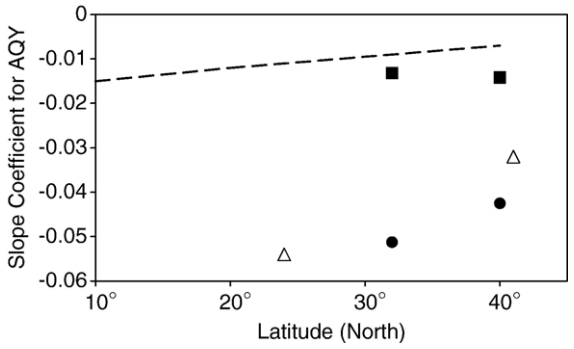

Fig. 8. Log-linear slope of AQY spectra vs. latitude (adapted from Zafiriou et al., 2003). The negative values indicate that photoproduction is more efficient at short wavelengths. Long wavelength AQY spectra slope coefficients from Zafiriou et al. (2003) [dashed line] and this study [closed squares]. Short wavelength AQY spectra slope coefficients from Zafiriou [open triangles] and this work [closed circles] (see text for explanation).

slope using the "two-segment" treatment (Fig. 8). However, slope coefficients for the longer-wavelength segment of Zafiriou et al.'s "two-segment" treatment became much less negative when moving northward. At 40° N in the Pacific, the slope coefficient for AQY spectra fit to wavelengths greater than 360 nm was −0.0229 in Zafiriou et al. (2003), which is of the same magnitude as the slope coefficient for the second exponential in our two-part aggregate AQY spectrum fit to the longer wavelengths: −0.0142 (Eq. (11)).

To determine the validity of using one AQY spectrum to predict the photochemical efficiency of carbon monoxide in different water types, our two part aggregate AQY spectrum, together with measured a_{CDOM} and E_o spectra for each experiment, was used to calculate CO production in each sample tube using Eq. (4). These predicted rates were consequently compared to the actual measured CO production data for our samples from coastal, near coastal and offshore waters (as divided in Table 1). For the coastal and shelf waters, the two-part aggregate AQY spectrum described the CO production in each cell as precisely as the sample-specific, single exponential AQY spectrum (Fig. 9a). However, for the offshore station the aggregate AQY underestimates the measured production for most points (Fig. 9c). Since the tubes with the lowest production (those under the longer wavelength cut-off filters) are well predicted by the aggregate, this suggests that the longer wavelength portion of the aggregate AQY is not where this discrepancy arises. It arises from the shorter wavelength production, suggesting that offshore waters may have a different AQY spectrum for the shorter wavelengths. Although there was no evidence of spatial variability of the single exponential AQY (as discussed above) the inability of the two-part aggregate AQY spectrum to reproduce the experimental data for blue water samples suggests that the offshore data might be better predicted by a specific AQY spectrum tuned for that environment.

The different efficiencies, for longer and shorter wavelengths, could reflect mechanistic or source material differences. It is thought that CO is formed by at least two mechanisms: dioxygen independent direct photolysis of carbonyl precursors that are present in CDOM at the start of irradiation and direct photolysis of precursors that form via light initiated auto-oxidation of the CDOM after the irradiation is started (Redden, 1982; Gao and Zepp, 1998). Although the efficiency of CO photoproduction has been shown to be higher in humic substances (e.g. Valentine and Zepp, 1993) than marine waters (Kettle, 1994; this study), the reaction mechanisms may be similar. The

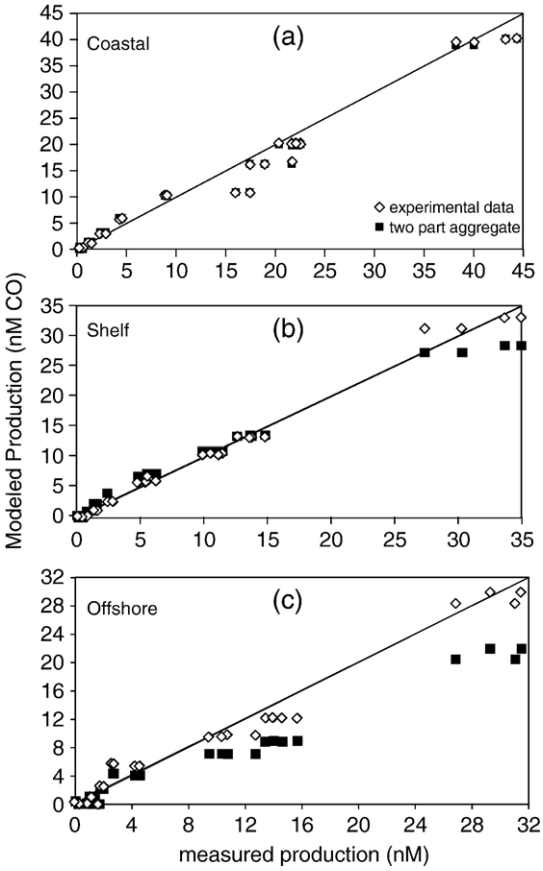

Fig. 9. Calculated versus measured CO production in irradiation cells for all Gulf of Maine stations. The solid line represents the one-to-one fit line for measured production. Calculated values used the experiment-specific irradiance and absorbance measurements with either the experiment specific quantum yield spectrum (diamonds) or the two-part exponential aggregate quantum yield spectrum (squares).

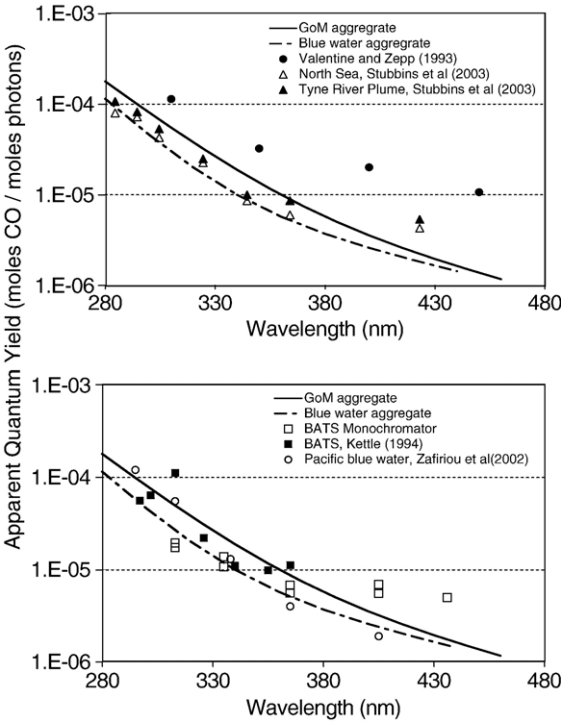

Fig. 10. Comparison of CO quantum yield spectra determined in this work ("GoM" aggregate and "Blue water" aggregate) to CO quantum yield spectra from other studies. Valentine and Zepp (1993) data presented in this figure are the average of quantum yields presented in their paper. The CO quantum yield from Kettle (1994) presented here is the 'measured CDOM BATS' sample using the measured absorption spectrum and water originating from the Sargasso Sea. The quantum yield presented as "Pacific blue water" is from Zafiriou et al. (2003) and represents the average along a North–South transect at 140° W. North Sea and Tyne River Plume CO AQY are from Stubbins (in press). All AQY spectra presented here, except for the aggregate spectra, were determined using monochromatic irradiation systems. In panel (b), the "BATS monochrometer" data was determined using the same sample as for our "Blue water" aggregate spectrum.

source of the absorbing material could also be causing different photochemical efficiencies.

3.5. Monochromatic verification of the method

As is the case in almost all aquatic environmental studies, it is very difficult to perform a rigorous comparison between results from different methodology (here, multispectral versus monochromatic irradiations) performed on different samples taken in different oceans at different times. This prompted us to make a direct comparison between a CO AQY spectrum determined using the more traditional monochromatic approach and our AQY results using the polychromatic method on an identical, fresh Sargasso Sea water sample. Duplicate water samples were collected at 20 m depth from the BATS station (32.0° N 64.5° W) and the AQY spectrum for CO photoproduction was determined using both a monochromatic light system (Andrews et al., 2000) and the polychromatic system used in this study. Similar to the method used to determine the Gulf of Maine aggregate AQY spectrum, a two-part AQY spectrum was calculated for the Sargasso Sea (designated "Blue water" in Fig. 10):

$$\phi(\lambda) = e^{(-(9.688+0.0513(\lambda-290)))} + e^{(-(11.507+0.0131(\lambda-290)))}. \quad (12)$$

Huixiang Xie (Université du Québec à Rimouski) performed the monochromatic experiments and subsequent quantum yield calculations. Of the monochromatic data, the two data points beyond 400 nm in the monochromatic irradiation are to be 'used with caution' (personal communication, Xie), since absorption coefficient measurements at the longer wavelengths were difficult to obtain and may be in error. Although the monochromatic AQY data are generally in good agreement with our two-part Sargasso Sea AQY spectrum (Fig. 10) when the two questionable points are removed, the monochromatic AQY is slightly lower in magnitude at the more energetic wavelengths (e.g.: 305 nm). Relating the differences in these two AQYs to previous comparisons made here, the monochromatic CO AQY would predict there to be slightly less CO produced under direct sunlight than would our AQY spectrum determined from the multispectral irradiation data. However, over the UV-A spectral range known to be most critical to CO photoproduction in sunlight (Valentine and Zepp, 1993), the comparison proves that both methods give almost identical results.

The two-part aggregate AQY spectrum for the Gulf of Maine presented here also compares well with previous studies (Fig. 10), at wavelengths less than 380 nm. The two-part aggregate AQY spectrum determined in the Gulf of Maine (Eq. (11)) is generally higher than the AQY determined in the Sargasso Sea (Eq. (12)) and is lower than the AQY spectrum published by Valentine and Zepp (1993) for numerous freshwater samples, which may suggest that terrestrial CDOM is more efficient at producing CO than marine derived CDOM. Thus when making generalized CO calculations, the Gulf of Maine aggregate AQY spectrum would be the appropriate AQY spectrum to use for coastal waters, while for the open ocean, the two-part Sargasso Sea AQY spectrum would be appropriate. In light of our limited comparison between the monochromatic and polychromatic irradiations of a single sample, these

methods appear to produce comparable carbon monoxide AQY spectra.

4. Summary

This work presents CO quantum yield spectra determined for different water types in the Northwest Atlantic, as well as the first published direct comparison of CO quantum yield spectra determined using a polychromatic irradiation system to those determined using a monochromatic irradiation system performed on the same water sample at sea. The aim of this study was twofold: to accumulate a new data set for CO AQY spectra to examine variability in different water types on fresh samples at sea and to verify our polychromatic irradiation technique for determination of CO AQY spectra. Despite the geographical and optical variability of 19 quantum yield spectra measured in the Gulf of Maine and the Northwest Atlantic Ocean, no significant spatial variability of the AQY spectra could be determined. A single AQY spectrum for CO photoproduction was calculated by pooling all of our experimental data for multispectral irradiation experiments for all stations, using a two-part exponential equation (termed "aggregate quantum yield"). This aggregate AQY spectrum is of a similar magnitude and shape as those previously published for CO AQY spectra. The direct comparison of AQY spectra determined for a single Sargasso Sea sample using both our multispectral statistical approach and a monochromatic system were found to produce comparable results.

Acknowledgements

The authors would like to thank D.J. Kieber, O.C. Zafiriou, the captain and crew of the *R/V* Endeavor, P. Kuhn, R.F. Davis, S. Beaupre, H. Xie and N. Nelson for technical assistance and J.J. Cullen for discussions of the manuscript. This work was supported by the Office of Naval Research grant N00014-96-1-0408 to Dalhousie University.

References

Amon, R.M.W., Opsahl, S., Benner, R., 1999. Major flux of terrigenous dissolved organic matter through the Arctic Ocean. Limnology and Oceanography 44 (8), 2017–2023.

Andrews, S.S., Caron, S., Zafiriou, O.C., 2000. Photochemical oxygen consumption in marine waters: a major sink for colored dissolved organic matter? Limnology and Oceanography 45 (2), 267–277.

Blough, N.V., Del Vecchio, R., 2002. Chromophoric dissolved organic matter (CDOM) in the coastal environment. In: Hansell, D.A., Carlson, C.A. (Eds.), Biogeochemistry of Marine Dissolved Organic Matter. Academic Press, San Diego, CA, pp. 509–546.

Braslavsky, S.E., Houk, K.N., Verhoeven, J.W., 1996. Glossary of Terms Used in Photochemistry, 2nd ed. International Union of Pure and Applied Chemistry, Amsterdam.

Conrad, R., Seiler, W., Bunse, G., Giehl, H., 1982. Carbon monoxide in seawater (Atlantic Ocean). Journal of Geophysical Research 87 (C11), 8839–8852.

Cullen, J.J., Neale, P.J., 1997. Biological weighting functions for describing the effects of ultraviolet radiation on aquatic systems. In: Häder, D.-P. (Ed.), The Effects of Ozone Depletions on Aquatic Ecosystems. R.G. Landes Company, Austin, TX, pp. 97–118.

Gao, H., Zepp, R.G., 1998. Factors influencing photoreactions of dissolved organic matter in a coastal river of the southeastern United States. Environmental Science and Technology 32, 2940–2946.

Gregg, W.W., Carder, K.L., 1990. A simple solar irradiance model for cloudless maritime atmospheres. Limnology and Oceanography 35 (8), 1657–1675.

Hu, C., Muller-Karger, F.E., Zepp, R.G., 2002. Absorbance, absorption coefficient, and apparent quantum yield: a comment on common ambiguity in the use of these optical concepts. Limnology and Oceanography 47 (4), 1261–1267.

Johannessen, S.C., Miller, W.L., 2001. Quantum yield for the photochemical production of dissolved inorganic carbon in the ocean. Marine Chemistry 76, 271–283.

Jones, R.D., 1991. Carbon monoxide and methane distribution and consumption in the photic zone of the Sargasso Sea. Deep-Sea Research 38, 625–635.

Kettle, A.J., 1994. A model for the temporal and spatial distribution of carbon monoxide in the mixed layer. M.Sc. Thesis, MIT/WHOI Joint Program, Woods Hole, MA, 146 pp.

Miller, W.L., Moran, M.A., Sheldon, W.M., Zepp, R.G., Opsahl, S., 2002. Determination of apparent quantum yield spectra for the formation of biologically labile photoproducts. Limnology and Oceanography 47 (2), 343–352.

Ohta, K., 1997. Diurnal variations of carbon monoxide concentration in the equatorial Pacific upwelling region. Journal of Oceanography 53, 173–178.

Opsahl, S., Benner, R., 1998. Photochemical reactivity of dissolved lignin in river and ocean waters. Limnology and Oceanography 43, 1297–1304.

Redden, G.D., 1982. Characteristics of photochemical production of carbon monoxide in seawater. M.Sc. Thesis, Oregon State University, Corvallis, OR, unpublished.

Rundel, R.D., 1983. Action spectra and estimation of biologically effective UV radiation. Physiologia Plantarum 58, 360–366.

Stubbins, A.P., 2001. Aspects of aquatic CO photoproduction from CDOM. Ph.D. Thesis, University of Newcastle, Newcastle Upon Tyne, UK.

Swinnerton, J.W., Linnenbo, V.J., Lamontag, R.A., 1970. Ocean: a natural source of carbon monoxide. Science 167 (3920), 984–986.

Valentine, R.L., Zepp, R.G., 1993. Formation of carbon monoxide from the photodegredation of terrestrial dissolved organic carbon in natural waters. Environmental Science and Technology 27, 409–412.

Vodacek, A., Blough, N.V., DeGrandpre, M.D., Peltzer, E.T., Nelson, R.K., 1997. Seasonal variation of CDOM and DOC in the Middle Atlantic Bight: terrestrial inputs and photoxidation. Limnology and Oceanography 42 (4), 674–686.

Wiesenburg, D.A., Guinasso, N.L., 1979. Equilibrium solubilities of methane, carbon monoxide and hydrogen in water and seawater. Journal of Chemical and Engineering Data 24 (4), 356–360.

Xie, H., Andrews, S.S., Martin, W.R., Miller, J., Ziolkowski, L., Taylor, C.D., Zafiriou, O.C., 2002. Validated methods for sampling

and headspace analysis of carbon monoxide in seawater. Marine Chemistry 77 (2–3), 93–108.

Zafiriou, O.C., Joussot-Dubien, J., Zepp, R.G., Zika, R.G., 1984. Photochemistry of natural waters. Environmental Science and Technology 18, 358A–371A.

Zafiriou, O.C., Andrews, S.S., Wang, W., 2003. Concordant estimates of oceanic carbon monoxide source and sink processes in the Pacific yield a balanced global 'blue-water' CO budget. Global Biogeochemical Cycles 17 (1), 1015.